



Research article

Dissipative Williamson fluid flow with double diffusive Cattaneo-Christov model due to a slippery stretching sheet embedded in a porous medium

W. Abbas^{1,*}, Ahmed M. Megahed², Osama M. Morsy¹, M. A. Ibrahim^{3,4} and Ahmed A. M. Said^{3,4}

¹ Basic and Applied Science Department, College of Engineering and Technology, Arab Academy for Science, Technology and Maritime Transport, Cairo, Egypt

² Department of Mathematics, Faculty of Science, Benha University, Benha, Egypt

³ Engineering Physics and Mathematics Department, Faculty of Engineering at El-Mattaria, Helwan university, Cairo, Egypt

⁴ Egyptian Academy of Engineering and Advanced Technology Affiliated to Ministry of Military Production, Cairo, Egypt

* **Correspondence:** Email: wael_abass@aast.edu; Tel: +201001395551.

Abstract: A numerical analysis of the incompressible two-dimensional flow of a non-Newtonian Williamson fluid is offered by expanding the sheet embedded in a porous medium and combining it with the Cattaneo-Christov model. Additionally, it is considered that the thermal conductivity and fluid viscosity both change as a linear function of temperature and an exponential function, respectively. The velocity, temperature and concentration field are all affected by thermal radiation, viscous dissipation, fluid variable properties, chemical reactions, and the slip velocity phenomenon. When the appropriate variables are employed, a system of non-linear, non-dimensional parameters emerges. The shooting method is used to numerically address this system. To better comprehend the impact of dimensionless parameters on dimensionless velocity, concentration, and temperature profiles, physical descriptions are prepared and justified using graphical representations. The values of the local skin-friction coefficient, the rate of heat transfer, and the rate of mass transfer are also investigated using tables. The behavior of changing fluid properties, on the other hand, establishes the link between Williamson fluid flow and the rate of heat mass transfer. According to the results, increasing the slip velocity and viscosity factors lowers both the Nusselt number and the Sherwood number. Also, due to an increase in Deborah number and the chemical reaction parameter, the temperature profiles decrease.

Keywords: Cattaneo-Christov model; Williamson fluid; porous medium; viscous dissipation; variable fluid properties

Mathematics Subject Classification: 65L10, 76A05, 76D50, 76S05

Nomenclature

a	coefficient of velocity
c_p	specific heat at constant pressure
C	nanoparticles concentration
Cf_x	skin friction coefficient
C_w	concentration of the fluid at the surface
C_∞	ambient concentration
D	the diffusion coefficient
De_1	the thermal Deborah number
De_2	the Deborah number of concentration field
Ec	the Eckert number
f	dimensionless stream function
j	the mass flux
k	permeability of porous medium
k_1	the rate of chemical reaction
k^*	mean absorption coefficient
K	chemical reaction parameter
Nu_x	local Nusselt number
Pr	Prandtl number
q	the heat flux
q_r	radiative heat flux
R	radiation parameter
Re	local Reynolds number
Sc	Schmidt number
Sh_x	the local Sherwood number
T	the temperature of the fluid
T_w	sheet temperature
T_∞	fluid temperature away the sheet
u	the component of the velocity in the x - direction
v	the component of the velocity in the y - direction
We	the local Weissenberg number
x, y	Cartesian coordinates

Greek symbols

μ	the viscosity coefficient
μ_∞	the ambient viscosity
ρ	the fluid density
ρ_∞	the ambient fluid density
α	the viscosity parameter
γ_1	the relaxation time for heat flux
γ_2	the relaxation time for mass flux
Γ	Williamson parameter
κ	the fluid thermal conductivity
ε	thermal conductivity parameter

ϕ	dimensionless fluid concentration
θ	dimensionless fluid temperature
λ_1	slip velocity factor
λ	slip velocity parameter
ν	the kinematic viscosity
ν_∞	the ambient kinematic viscosity
Δ	the porous parameter
η	similarity variable
σ^*	Stefan-Boltzmann constant

Superscripts

'	differentiation with respect to η
w	wall condition
∞	free stream condition

1. Introduction

Fluids can be categorized into Newtonian and non-Newtonian categories based on shear stress, according to the rheological behavior presented earlier [1]. The linear relationship between stress and strain identifies the Newtonian type. Physical problems involving Newtonian fluids have piqued the interest of scientists and engineers in recent years [2–6]. Unlike Newtonian fluids, the non-Newtonian fluid's viscosity does not remain constant with the shear rate and can be affected by a variety of factors. Slurries, foams, polymer melts, emulsions, and solutions are examples of non-Newtonian fluids. Non-Newtonian fluids have been extensively researched due of their numerous industrial applications. Furthermore, given the wide range of fluids of interest, heat transfer with non-Newtonian fluids is a vast topic that cannot be treated in its entirety in this study. Paint and adhesives industries, nuclear reactors, cooling systems, and drilling rigs are all examples of non-Newtonian fluid applications. To discover applications in new sectors, non-Newtonian fluid flows need a full investigation in terms of analytical, experimental, and numerical features. A variety of models have been used to explain non-Newtonian fluids in a number of works [7–20]. Non-Newtonian fluids were examined further by Megahed [7] and Ahmed and Iqba [8] for the power-law model; Cortell [9], Midya [10] and Megahed [11] for the viscoelastic model; Ibrahim and Hindebu [12], Bilal and Ashbar [13] and Abbas and Megahed [14] for the Powell-Eyring model; Pramanik [15], Rana et al. [16] and Alali and Megahed [17] for the Casson model; and Hayat et al. [18], Prasad et al. [19] and Megahed [20] for the Maxwell model. It is important to note that this study considers the viscous dissipation phenomenon. Only if the friction increases to the point where the fluid temperature field is noticeably warmed should this phenomenon be taken into account. There is a vast amount of information accessible on the viscous dissipation phenomenon and many fluid flow models [21–23].

The Cattaneo-Christov heat transfer model is a modified form of the Fourier law that is used to calculate the characteristics of a heat flux model while considering the relaxation time for heat flux

dispersion across the physical model [24]. As a result, several researchers [25–30] have conducted more research on this model's most essential characteristics. In many industrial and technical sectors, including natural processes, biomedical engineering, chemical engineering and petroleum engineering, the Cattaneo-Christov heat transfer model makes the heat transfer mechanism and fluid flow in porous media crucially important [31]. So, the cooling process, which is one of the benefits, is one of the most important real life applications of our research, especially in light of the influence of the double diffusive Cattaneo-Christov model on the non-Newtonian Williamson model. Also, this benefit can lower the cost of the finished product and serve as the primary component in preventing product fault. In addition, the novelty of the current work is to examine how Cattaneo-Christov heat mass fluxes affect non-Newtonian dissipative Williamson fluids due to a slippery stretching sheet under the presence of thermal radiation, chemical reactions, and changing thermal characteristics.

2. Basic governing equations

Consider the flow of a non-Newtonian Williamson fluid with the Cattaneo-Christov phenomenon in two dimensions. It is assumed that the stretched sheet, which is embedded in a porous medium with permeability k , is what causes the fluid to flow. Likewise, it is considered that the fluid concentration along the sheet is C_w and that the sheet at $y = 0$ is heated with temperature T_w . The fluid is flowing in a streamlined pattern, and its viscosity is low but not negligible. The modifying impact appears to be restricted within a narrow layer adjacent to the sheet surface; this is called the boundary layer region. Within such a layer, the fluid velocity rapidly changes from its starting value to its mainstream value. We chose this model because it can accurately describe a large number of non-Newtonian fluids, possibly the majority, over a vast scope of shear rates. The x -axis is chosen parallel to the surface of the sheet in the flow direction, with the origin at the sheet's leading edge, and the y -axis is perpendicular to it (Figure 1). Let T be the Williamson fluid temperature and u and v be the x -axial and perpendicular velocity components, respectively.

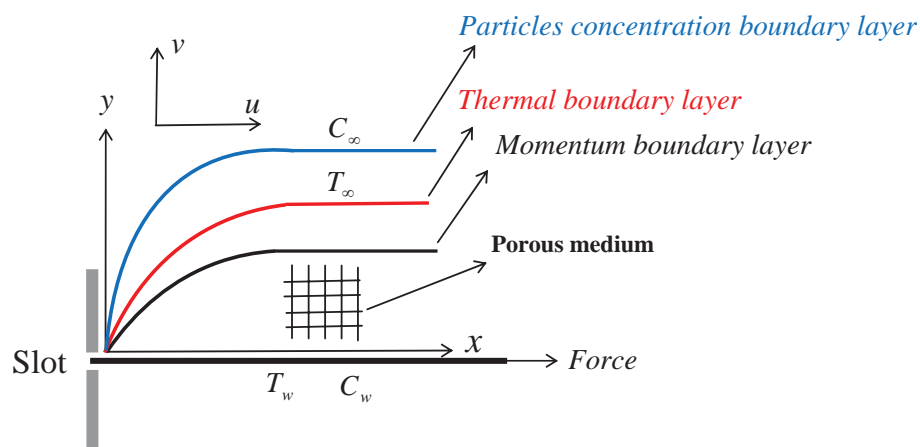


Figure 1. A physical diagram of a boundary layer slip flow system.

The sheet on which the slip velocity phenomenon occurs is supposed to be rough and exposed to thermal radiation with a radiative heat flux of q_r . The concept of the slip phenomenon was put forth by

Mahmoud [32], who proved that it linearly depends on the shear stress τ_w at the surface, i.e.,

$$u - U_w = \lambda^* \tau_w, \quad (2.1)$$

where $\tau_w = \left[\mu \frac{\partial u}{\partial y} + \mu \frac{\Gamma}{\sqrt{2}} \left(\frac{\partial u}{\partial y} \right)^2 \right]_{y=0}$ and U_w is the fluid velocity at the sheet. Also, chemical reactions and the viscous dissipation phenomenon are taken into consideration in this study. Similarly, the temperature T_w and concentration C_w are constant on the sheet. We continue to assume that the Williamson fluid thermal conductivity varies linearly with temperature $\kappa = \kappa_\infty(1 + \varepsilon\theta)$ [33], although its viscosity varies nonlinearly with temperature as $\mu = \mu_\infty e^{-\alpha\theta}$ [33], where μ_∞ is the Williamson fluid's viscosity at ambient temperature, α is the viscosity parameter, κ_∞ is the liquid thermal conductivity at ambient temperature, and ε is the thermal conductivity parameter. According to the aforementioned hypotheses, the fundamental equations governing the flow are

$$\nabla \cdot \underline{U} = 0, \quad (2.2)$$

$$\rho_\infty (\underline{U} \cdot \nabla) \underline{U} = -\nabla p + \nabla \cdot \underline{\tau} + \underline{r}, \quad (2.3)$$

$$\rho_\infty c_p (\underline{U} \cdot \nabla) T = -\nabla \cdot q - \nabla \cdot q_r + \Phi, \quad (2.4)$$

$$(\underline{U} \cdot \nabla) C = -\nabla \cdot j - k_1 (C - C_\infty), \quad (2.5)$$

where $\underline{U} = (u, v, 0)$, p is the pressure, $\underline{r} = \frac{-\mu}{k} \underline{U}$ is the Darcy impedance for a Williamson fluid, Φ is the function of dissipation, q is the heat flux, and j is the mass flux. Also, the heat flux q and the mass flux j satisfy the following relations, respectively [34]:

$$q + \gamma_1 (\underline{U} \cdot \nabla q - q \cdot \nabla \underline{U}) = -\kappa \nabla T, \quad (2.6)$$

$$j + \gamma_2 (\underline{U} \cdot \nabla j - j \cdot \nabla \underline{U}) = -D \nabla C. \quad (2.7)$$

Then, using the conventional boundary layer approximation, we can show that the equations below control the flow and heat mass transfer in our physical description [35].

$$\frac{\partial u}{\partial x} + \frac{\partial v}{\partial y} = 0, \quad (2.8)$$

$$u \frac{\partial u}{\partial x} + v \frac{\partial u}{\partial y} = \frac{1}{\rho_\infty} \frac{\partial}{\partial y} \left\{ \mu \frac{\partial u}{\partial y} + \mu \frac{\Gamma}{\sqrt{2}} \left(\frac{\partial u}{\partial y} \right)^2 \right\} - \frac{\mu}{\rho_\infty k} u, \quad (2.9)$$

$$u \frac{\partial T}{\partial x} + v \frac{\partial T}{\partial y} + \gamma_1 \Omega_E = \frac{1}{\rho_\infty c_p} \frac{\partial}{\partial y} \left(\kappa \frac{\partial T}{\partial y} \right) - \frac{1}{\rho_\infty c_p} \frac{\partial q_r}{\partial y} + \frac{\mu}{\rho_\infty c_p} \left\{ \left(\frac{\partial u}{\partial y} \right)^2 + \frac{\Gamma}{\sqrt{2}} \left(\frac{\partial u}{\partial y} \right)^3 \right\} \quad (2.10)$$

$$u \frac{\partial C}{\partial x} + v \frac{\partial C}{\partial y} + \gamma_2 \Omega_C = D \frac{\partial^2 C}{\partial y^2} - k_1 (C - C_\infty). \quad (2.11)$$

In terms of boundary conditions, the fluid flow model is subjected to the following [36]:

$$u = ax + \frac{\lambda_1}{\mu_\infty} \left(\mu \frac{\partial u}{\partial y} + \mu \frac{\Gamma}{\sqrt{2}} \left(\frac{\partial u}{\partial y} \right)^2 \right), \quad v = 0, \quad T = T_w, \quad C = C_w \quad \text{at} \quad y = 0, \quad (2.12)$$

$$u \rightarrow 0, \quad T \rightarrow T_\infty, \quad C \rightarrow C_\infty, \quad \text{at } y \rightarrow \infty, \quad (2.13)$$

where

$$\Omega_E = u^2 \frac{\partial^2 T}{\partial x^2} + v^2 \frac{\partial^2 T}{\partial y^2} + u \frac{\partial u}{\partial x} \frac{\partial T}{\partial x} + v \frac{\partial v}{\partial y} \frac{\partial T}{\partial y} + u \frac{\partial v}{\partial x} \frac{\partial T}{\partial y} + v \frac{\partial u}{\partial y} \frac{\partial T}{\partial x} + 2uv \frac{\partial^2 T}{\partial x \partial y}, \quad (2.14)$$

$$\Omega_C = u^2 \frac{\partial^2 C}{\partial x^2} + v^2 \frac{\partial^2 C}{\partial y^2} + u \frac{\partial u}{\partial x} \frac{\partial C}{\partial x} + v \frac{\partial v}{\partial y} \frac{\partial C}{\partial y} + u \frac{\partial v}{\partial x} \frac{\partial C}{\partial y} + v \frac{\partial u}{\partial y} \frac{\partial C}{\partial x} + 2uv \frac{\partial^2 C}{\partial x \partial y}. \quad (2.15)$$

In addition, ρ_∞ represents the ambient density, and μ represents the Williamson viscosity. Γ stands for a Williamson time constant, k is the permeability of the porous medium, c_p signifies the specific heat at constant pressure, k_1 is the reaction rate, D is the diffusion coefficient, γ_1 is the time it takes for the heat flux to relax, γ_2 is the time it takes for the mass flux to relax, and C_∞ is the ambient fluid concentration. Now, we utilize suitable similarity transforms, such as [35]:

$$u = axf'(\eta), \quad v = -\sqrt{av_\infty}f(\eta), \quad \eta = y\sqrt{\frac{a}{v_\infty}}, \quad \theta(\eta) = \frac{T - T_\infty}{T_w - T_\infty}, \quad \phi(\eta) = \frac{C - C_\infty}{C_w - C_\infty}. \quad (2.16)$$

When the last postulate is taken into account, Equation (2.8) is consequently confirmed, and the other equations are reduced to the following form:

$$\left((1 + W_e f'') f''' - \alpha \theta' f'' \left(1 + \frac{W_e}{2} f'' \right) \right) e^{-\alpha \theta} - f'^2 + f f'' - \Delta e^{-\alpha \theta} f' = 0, \quad (2.17)$$

$$\frac{1}{Pr} \left((1 + R + \varepsilon \theta) \theta'' + \varepsilon \theta'^2 \right) + f \theta' - De_1 (f f' \theta' + f^2 \theta'') + Ec \left(f'^2 + \frac{W_e}{2} f''^3 \right) e^{-\alpha \theta} = 0, \quad (2.18)$$

$$\frac{1}{Sc} \phi'' + f \phi' - De_2 (f f' \phi' + f^2 \phi'') - K \phi = 0. \quad (2.19)$$

The relevant physical boundary conditions are also modified as a result of the invocation of the prior dimensionless transformations as

$$f = 0, \quad f' = 1 + \lambda \left(f'' + \frac{W_e}{2} f''^2 \right) e^{-\alpha \theta}, \quad \theta = 1, \quad \phi = 1 \quad \text{at } \eta = 0, \quad (2.20)$$

$$f' \rightarrow 0, \quad \theta \rightarrow 0, \quad \phi \rightarrow 0 \quad \text{at } \eta \rightarrow \infty. \quad (2.21)$$

The dimensionless controlling factors that have emerged are the local Weissenberg number $W_e = \Gamma x \sqrt{\frac{2a^2}{v_\infty}}$, the porous parameter $\Delta = \frac{v_\infty}{ak}$, the radiation parameter $R = \frac{16\sigma^* T_\infty^3}{3k^* \kappa_\infty}$, the slip velocity parameter $\lambda = \lambda_1 \sqrt{\frac{a}{v_\infty}}$, the thermal Deborah number $De_1 = \gamma_1 a$, the Eckert number $Ec = \frac{u_w^2}{c_p(T_w - T_\infty)}$, the Deborah number which related to the mass transfer field $De_2 = \gamma_2 a$, the chemical reaction parameter $K = \frac{k_1}{a}$ and the Prandtl number $Pr = \frac{\mu_\infty c_p}{\kappa_\infty}$. It is interesting to see that when $W_e = 0$, the nature of the non-Newtonian Williamson fluid model transforms into a Newtonian fluid model.

Furthermore, the local Nusselt number Nu_x , the local Sherwood number Sh_x , and the drag force coefficient in terms of Cf_x are determined by [37]:

$$Cf_x Re^{\frac{1}{2}} = - \left(f''(0) + \frac{W_e}{2} f''^2(0) \right) e^{-\alpha \theta(0)}, \quad \frac{Nu_x Re^{\frac{1}{2}}}{1 + R} = -\theta'(0), \quad Sh_x Re^{\frac{1}{2}} = -\phi'(0), \quad (2.22)$$

where $Re = \frac{u_w x}{v_\infty}$ is the local Reynolds number.

3. Outcomes with discussion

Table 1 compares the values of the local skin-friction coefficient ($Cf_x Re^{\frac{1}{2}}$) with those from Andersson's earlier work [38] to validate the current findings acquired by the shooting technique. This comparison is carried out for various slip velocity parameter values. We can confidently state that our results are in good accord with those references based on this comparison. Furthermore, the collected results show that the proposed strategy is both reliable and efficient.

Table 1. Comparison of $Cf_x Re^{\frac{1}{2}}$ with the results of Andersson [38] when $W_e = \alpha = \Delta = 0$.

λ	Andersson [38]	Present work
0.0	1.0000	1.0000000000
0.1	0.8721	0.8720029514
0.2	0.7764	0.7763995210
0.5	0.5912	0.5911972051
1.0	0.4302	0.4301859007
2.0	0.2840	0.2839991098
5.0	0.1448	0.1447985799

The simulation studies of a non-Newtonian Williamson fluid over a stretching surface are presented in this section. The momentum field considers the slip velocity phenomenon, the energy equation includes the viscous dissipation and thermal radiation effects, and the mass transport equation includes the chemical process. Via the shooting approach, the governing equations are numerically solved using supported dimensionless transformation. All the governing physical parameters are utilized in the following ranges: $0.0 \leq \Delta \leq 0.5$, $0.0 \leq \alpha \leq 0.5$, $0.0 \leq \lambda \leq 0.4$, $0.0 \leq W_e \leq 0.5$, $0.0 \leq \varepsilon \leq 0.5$, $0.0 \leq De_1 \leq 0.4$, $0.0 \leq De_2 \leq 1.0$, $0.0 \leq K \leq 0.5$ and $0.0 \leq Ec \leq 0.5$. Thus, the values of the parameters with fixed values which are used for graphical display can be chosen as $\Delta = 0.2$, $W_e = 0.4$, $Sc = 4.0$, $R = 0.5$, $\alpha = 0.2$, $K = 0.2$, $\varepsilon = 0.2$, $\lambda = 0.2$, $De_1 = 0.2$, $Pr = 7.0$, $De_2 = 0.2$ and $Ec = 0.2$. This section discusses the graphical effects of physical dimensionless amounts on complicated profiles. The effect of porous parameter Δ on the Williamson fluid velocity is tested and introduced by means of Figure 2(a). When we assume $\Delta = 0.0, 0.2$ and 0.5 , both the velocity of the Williamson fluid and the thickness of the boundary layer are dramatically reduced. The porous parameter exhibits this behavior due to its direct presence in the velocity field. Figure 2(b) shows the impact of the porous parameter on both the fluid temperature and the fluid concentration. We discovered that the Williamson fluid temperature $\theta(\eta)$ rises as the porous parameter rises. Likewise, the Williamson fluid concentration $\phi(\eta)$ is subject to the same phenomenon. Physically, the porous parameter causes a restriction in the flow of the fluid, which reduces the fluid's velocity and raises the temperature and concentration distributions.

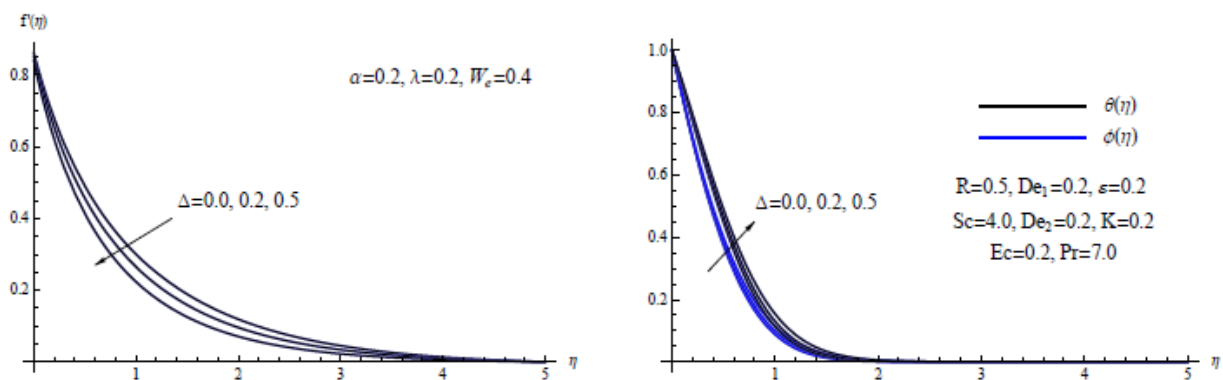


Figure 2. (a) $f'(\eta)$ for chosen Δ . (b) $\theta(\eta)$ and $\phi(\eta)$ for chosen Δ .

The velocity, temperature and concentration profiles for the viscosity parameter α are shown in Figure 3. It's worth noting that α has a greater impact on velocity profiles than on temperature or concentration profiles. Increases in the viscosity parameter α result in decreases in the velocity profile $f'(\eta)$ and associated boundary layer thickness, whereas the temperature $\theta(\eta)$ and concentration $\phi(\eta)$ fields show the opposite tendency. Physically, a barrier type of force will be produced in the Williamson flow due to the fluid viscosity's reliance on temperature. The fluid velocity can be slowed down by this force. The fluid layers consequently acquire little thermal energy via the same force.

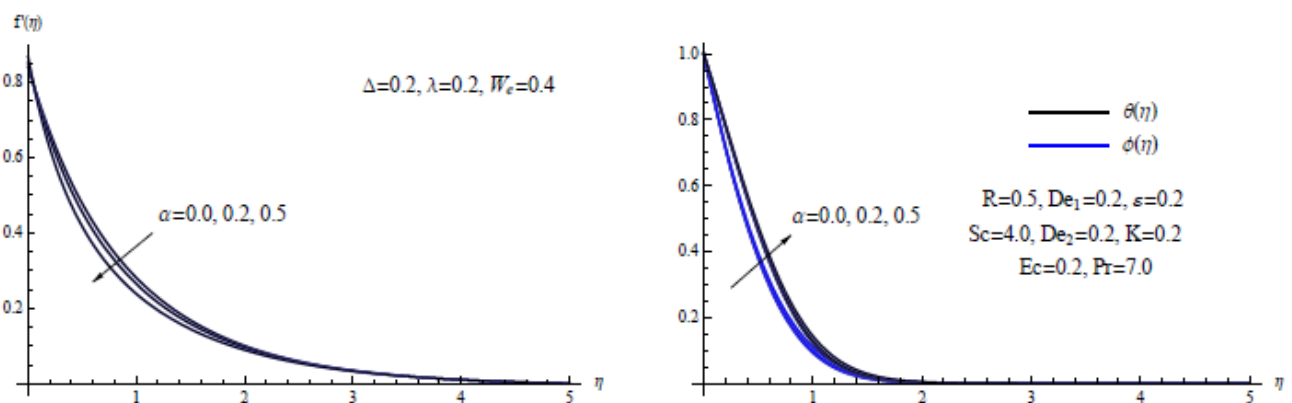


Figure 3. (a) $f'(\eta)$ for chosen α . (b) $\theta(\eta)$ and $\phi(\eta)$ for chosen α .

Figure 4 shows the velocity, temperature, and concentration for the slip velocity parameter λ . When the slip velocity parameter is increased, both the temperature $\theta(\eta)$ and concentration $\phi(\eta)$ profiles increase, and as a result, the thermal boundary layer thickness increases. With the same parameter, however, the reverse tendency is observed for both the velocity distribution $f'(\eta)$ and the sheet velocity $f'(0)$. In terms of physics, the existence of the slip phenomenon produces a resistance force between the fluid layers, which in turn reduces the fluid's velocity and enhances the fluid temperature.

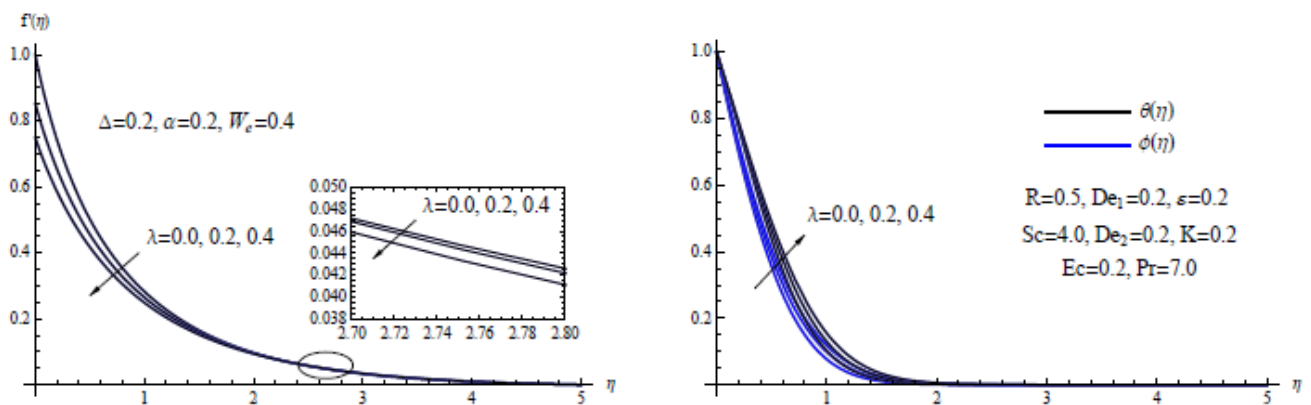


Figure 4. (a) $f'(\eta)$ for chosen λ . (b) $\theta(\eta)$ and $\phi(\eta)$ for chosen λ .

The influence of the local Weissenberg number W_e on Williamson fluid velocity, Williamson fluid temperature, and Williamson fluid concentration is depicted in Figure 5. The graph illustrates that raising the local Weissenberg number W_e causes temperature and concentration distributions to rise, whereas the same value of W_e causes fluid velocity to decrease. Physically, a high local Weissenberg number increases the viscous forces that hold the Williamson fluid layers together, which lowers the fluid's velocity and improves the fluid's heat distribution through the boundary layer.

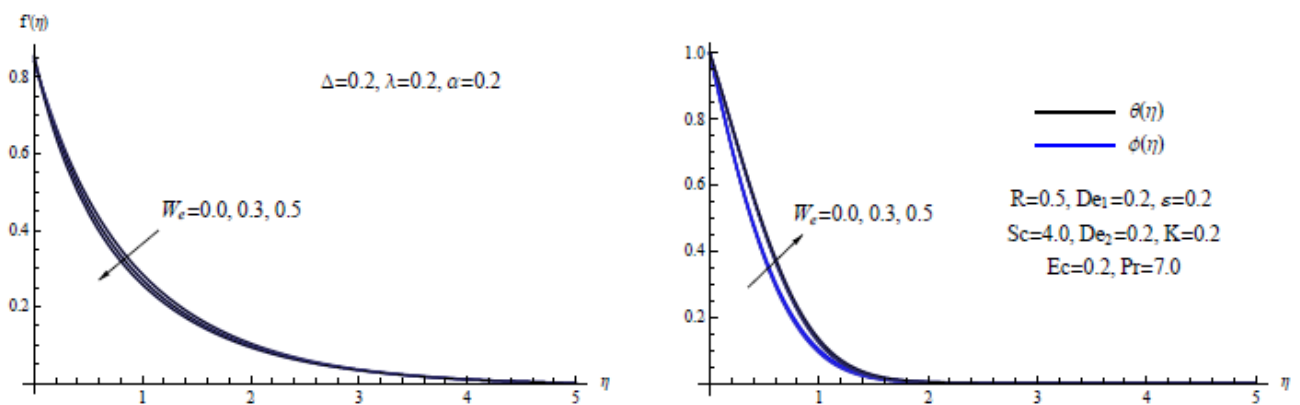


Figure 5. (a) $f'(\eta)$ for chosen W_e . (b) $\theta(\eta)$ and $\phi(\eta)$ for chosen W_e .

The impact of the thermal conductivity parameter ϵ has been depicted in Figure 6. The larger values of ϵ correspond to a broader temperature distribution $\theta(\eta)$ and a marginal increase in the concentration field $\phi(\eta)$, but an increase in the same parameter results in a slight decrease in the velocity graphs $f'(\eta)$. Physically, higher values of the thermal conductivity characteristic indicate a fluid's ability to gain higher temperatures, which may cause the fluid's temperature to rise through the thermal layer.

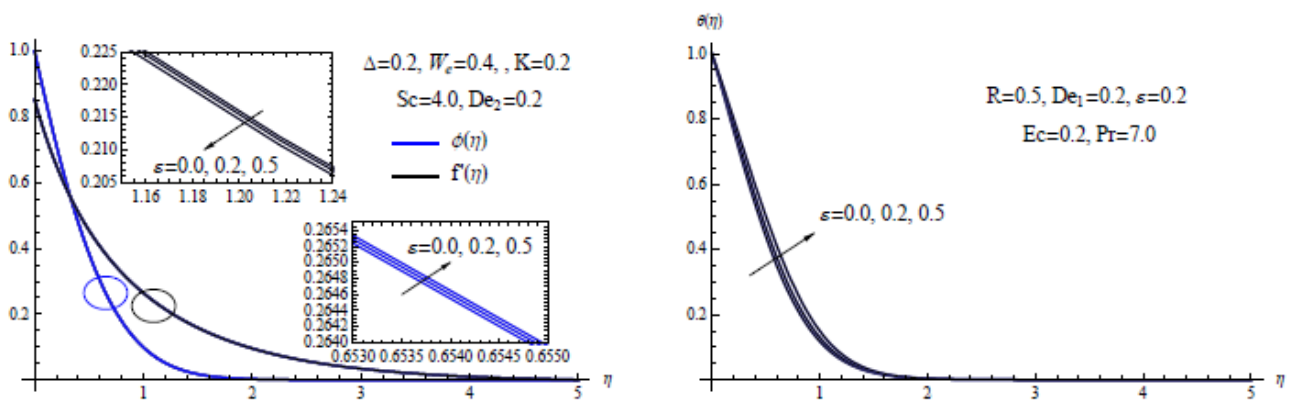


Figure 6. (a) $f'(\eta)$ and $\phi(\eta)$ for chosen ϵ . (b) $\theta(\eta)$ for chosen ϵ .

The effect of the thermal Deborah number De_1 on velocity distribution, temperature distribution and concentration distribution is depicted in Figure 7. The Deborah number is a rheological term that describes the fluidity of materials under specified flow circumstances. Low-relaxation-time materials flow freely and exhibit quick stress decay as a result. The fluid motion $f'(\eta)$ scarcely improves with the bigger De_1 parameter, but the concentration profiles $\phi(\eta)$ are slightly reduced. Furthermore, extended values of the thermal Deborah number De_1 reduce both the thickness of the thermal region and the profiles of temperature $\theta(\eta)$.

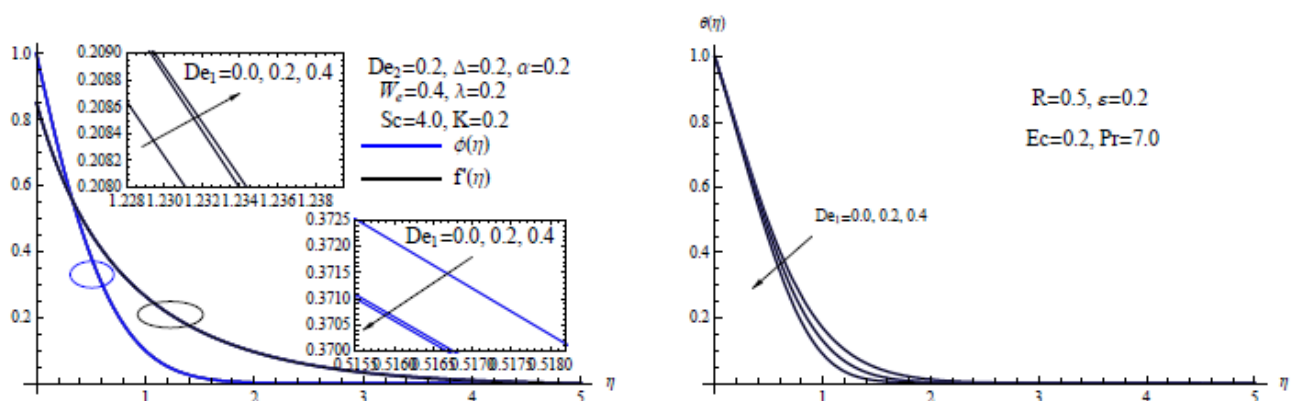


Figure 7. (a) $f'(\eta)$ and $\phi(\eta)$ for chosen De_1 . (b) $\theta(\eta)$ for chosen De_1 .

Figure 8 depicts the dimensionless velocity, dimensionless concentration, and thermal profiles for different Eckert number Ec estimates. It is evident that as the Eckert number is increased, the dimensionless velocities $f'(\eta)$ diminish modestly, while the dimensionless concentration $\phi(\eta)$ increases slightly. Furthermore, the increase in Eckert number Ec obviously increases both the temperature profile and the thickness of the thermal region. Physically, the Williamson fluid moves quickly, causing some kinetic energy to be transformed into thermal energy as a result of the viscous dissipation phenomenon. This promotes the fluid distributing heat more through the thermal layer.

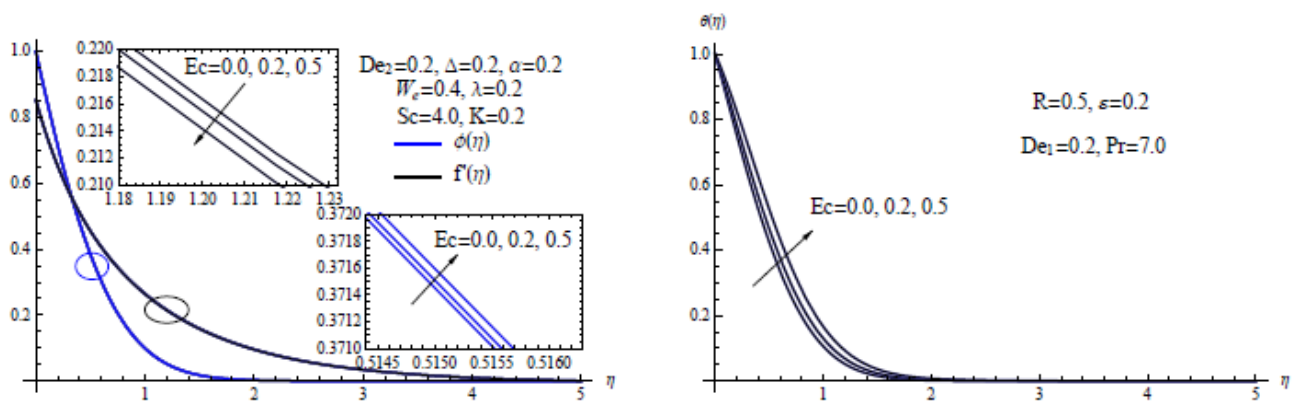


Figure 8. (a) $f'(\eta)$ and $\phi(\eta)$ for chosen Ec . (b) $\theta(\eta)$ for chosen Ec .

Figure 9 shows the effects of the Deborah number De_2 , which is related to mass transfer, and the chemical reaction parameter K on Williamson fluid concentration. Because both the concentration characteristics $\phi(\eta)$ and the concentration boundary thickness of the Williamson fluid decrease when both the chemical reaction parameter and the Deborah number increase, the mass transfer rate increases as well.

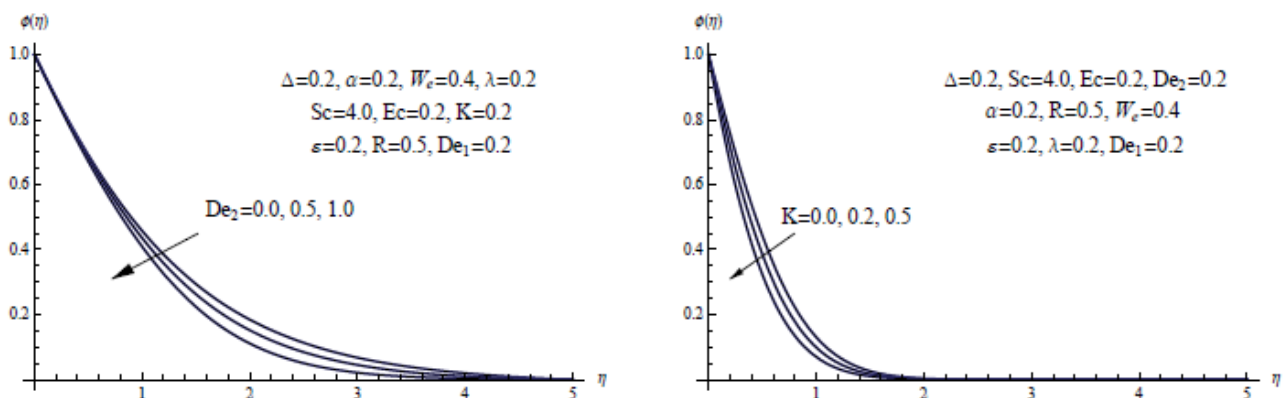


Figure 9. (a) $\phi(\eta)$ for chosen De_2 . (b) $\phi(\eta)$ for chosen K .

From an engineering standpoint, we now concentrate on the fluctuations of physical quantities of interest. For all regulating factors of our model, the local skin-friction $Cf_x(Re_x)^{\frac{1}{2}}$, the local Nusselt number $\frac{Nu_x Re_x^{-\frac{1}{2}}}{1+R}$, and the local Sherwood number $Sh_x Re_x^{-\frac{1}{2}}$ are introduced in Table 2. Skin friction coefficient values decrease when the viscosity parameter, slip velocity parameter, and local Weissenberg number increase, lowering both the local Nusselt number and the local Sherwood number. The skin friction coefficient and the local Nusselt number, respectively, grow and shrink uniformly with the thermal Deborah number and the Eckert number. Furthermore, increasing the chemical reaction parameter or the Deborah number increases the rate of mass transfer, while increasing the thermal conductivity parameter reduces it significantly.

Table 2. Values for $Cf_x(Re_x)^{\frac{1}{2}}$, $\frac{Nu_x Re_x^{-\frac{1}{2}}}{1+R}$ and $Sh_x Re_x^{-\frac{1}{2}}$ for various values of Δ , α , λ , ε , W_e , De_1 , Ec , De_2 and K with $Pr = 7.0$, $Sc = 4.0$ and $R = 0.5$.

Δ	α	λ	W_e	ε	De_1	Ec	De_2	K	$Cf_x(Re_x)^{\frac{1}{2}}$	$\frac{Nu_x Re_x^{-\frac{1}{2}}}{1+R}$	$Sh_x Re_x^{-\frac{1}{2}}$
0.0	0.2	0.2	0.4	0.2	0.2	0.2	0.2	0.2	0.693231	0.728441	1.549131
0.2	0.2	0.2	0.4	0.2	0.2	0.2	0.2	0.2	0.742281	0.691424	1.521591
0.5	0.2	0.2	0.4	0.2	0.2	0.2	0.2	0.2	0.804956	0.642281	1.485710
0.2	0.0	0.2	0.4	0.2	0.2	0.2	0.2	0.2	0.797036	0.703410	1.535110
0.2	0.2	0.2	0.4	0.2	0.2	0.2	0.2	0.2	0.742281	0.691424	1.521591
0.2	0.5	0.2	0.4	0.2	0.2	0.2	0.2	0.2	0.658089	0.670908	1.496560
0.2	0.2	0.0	0.4	0.2	0.2	0.2	0.2	0.2	0.902041	0.698173	1.604453
0.2	0.2	0.2	0.4	0.2	0.2	0.2	0.2	0.2	0.742281	0.691424	1.521591
0.2	0.2	0.4	0.4	0.2	0.2	0.2	0.2	0.2	0.629907	0.673791	1.458850
0.2	0.2	0.2	0.0	0.2	0.2	0.2	0.2	0.2	0.796081	0.705117	1.537281
0.2	0.2	0.2	0.3	0.2	0.2	0.2	0.2	0.2	0.758219	0.695903	1.526750
0.2	0.2	0.2	0.5	0.2	0.2	0.2	0.2	0.2	0.723105	0.685343	1.514782
0.2	0.2	0.2	0.4	0.0	0.2	0.2	0.2	0.2	0.743328	0.753634	1.521621
0.2	0.2	0.2	0.4	0.2	0.2	0.2	0.2	0.2	0.742281	0.691424	1.521591
0.2	0.2	0.2	0.4	0.5	0.2	0.2	0.2	0.2	0.740897	0.619058	1.521451
0.2	0.2	0.2	0.4	0.2	0.0	0.2	0.2	0.2	0.741341	0.667262	1.521580
0.2	0.2	0.2	0.4	0.2	0.2	0.2	0.2	0.2	0.742281	0.691424	1.521591
0.2	0.2	0.2	0.4	0.2	0.4	0.2	0.2	0.2	0.743587	0.716488	1.521622
0.2	0.2	0.2	0.4	0.2	0.2	0.0	0.2	0.2	0.744102	0.827635	1.521640
0.2	0.2	0.2	0.4	0.2	0.2	0.2	0.2	0.2	0.742281	0.691424	1.521591
0.2	0.2	0.2	0.4	0.2	0.2	0.5	0.2	0.2	0.739576	0.487913	1.521520
0.2	0.2	0.2	0.4	0.2	0.2	0.2	0.0	0.2	0.742281	0.691424	1.497912
0.2	0.2	0.2	0.4	0.2	0.2	0.2	0.5	0.2	0.742281	0.691424	1.559190
0.2	0.2	0.2	0.4	0.2	0.2	0.2	1.0	0.2	0.742281	0.691424	1.619098
0.2	0.2	0.2	0.4	0.2	0.2	0.2	0.2	0.0	0.742281	0.691426	1.238491
0.2	0.2	0.2	0.4	0.2	0.2	0.2	0.2	0.2	0.742281	0.691426	1.521591
0.2	0.2	0.2	0.4	0.2	0.2	0.2	0.2	0.5	0.742281	0.691426	1.872482

4. Conclusions

A description of the heat and mass transport features of a viscous non-Newtonian Williamson fluid across a stretching sheet that is embedded in a porous medium was attempted here. Heat and mass transfer in the Williamson fluid in the presence of thermal radiation, slip velocity, variable thermal characteristics, Cattaneo-Christov heat mass fluxes, chemical reaction and viscous dissipation are all investigated in this study. The governing equations have been converted via dimensionless transformations into a set of coupled nonlinear ordinary differential equations, which are then numerically solved using the shooting technique. The following are the major characteristics of the current work.

- 1) A concentration field grows as the viscosity and slip parameters increase, but as the chemical reactions and Deborah number increase, the concentration field decreases.
- 2) The Sherwood number decreases as the Eckert number rises, whereas the Deborah number and chemical parameter increase it.
- 3) The velocity profile is reduced by the viscosity and slip velocity parameters, whereas a minor increase in velocity profile occurs due to the Deborah number being increased.
- 4) The Deborah number has a lower temperature profile than the thermal conductivity parameter and the Eckert number.
- 5) The heat transfer rate is reduced by both the thermal conductivity parameter and the viscous dissipation phenomenon.
- 6) Skin-friction coefficient values increase with the porous parameter, but they decrease with an increase in either the slip velocity or the viscosity parameter.
- 7) When the local Weissenberg number is higher, both the skin-friction coefficient and the local Nusselt number's magnitude fall.

Acknowledgments

The authors are thankful to the honorable editor and anonymous reviewers for their useful suggestions and comments which improved the quality of this paper.

Conflict of interest

The authors declare that they have no competing interests.

References

1. A. Acrivos, A theoretical analysis of laminar natural convection heat transfer to non-Newtonian fluids, *AIChE J.*, **6** (1960), 584–590. <https://doi.org/10.1002/aic.690060416>
2. L. J. Crane, Flow past a stretching plate, *Z. Angew. Math. Phys.*, **21** (1970), 645–647. <https://doi.org/10.1007/BF01587695>
3. L. J. Grubka, K. M. Bobba, Heat transfer characteristics of a continuous stretching surface with variable temperature, *J. Heat Transfer*, **107** (1985), 248–250. <https://doi.org/10.1115/1.3247387>
4. I-C. Liu, A. M. Megahed, Numerical study for the flow and heat transfer in a thin liquid film over an unsteady stretching sheet with variable fluid properties in the presence of thermal radiation, *J. Mech.*, **28** (2012), 291–297. <https://doi.org/10.1017/jmech.2012.32>
5. A. M. Megahed, Variable heat flux effect on MHD flow and heat transfer over an unsteady stretching sheet in the presence of thermal radiation, *Can. J. Phys.*, **92** (2014), 86–91. <https://doi.org/10.1139/cjp-2012-0543>
6. M. S. Uddin, Viscous and joules dissipation on MHD flow past a stretching porous surface embedded in a porous medium, *J. Appl. Math. Phys.*, **3** (2015), 1710–1725. <https://doi.org/10.4236/jamp.2015.312196>

7. A. M. Megahed, Variable viscosity and slip velocity effects on the flow and heat transfer of a power-law fluid over a non-linearly stretching surface with heat flux and thermal radiation, *Rheol. Acta*, **51** (2012), 841–847. <https://doi.org/10.1007/s00397-012-0644-8>
8. F. Ahmed, M. Iqba, MHD power law fluid flow and heat transfer analysis through Darcy Brinkman porous media in annular sector, *Int. J. Mech. Sci.*, **130** (2017), 508–517. <https://doi.org/10.1016/j.ijmecsci.2017.05.042>
9. R. Cortell, Similarity solutions for flow and heat transfer of a viscoelastic fluid over a stretching sheet, *Int. J. Nonlin. Mech.*, **29** (1994), 155–161. [https://doi.org/10.1016/0020-7462\(94\)90034-5](https://doi.org/10.1016/0020-7462(94)90034-5)
10. S. K. Khan, Heat transfer in a viscoelastic fluid flow over a stretching surface with heat source/sink, suction/blowing and radiation, *Int. J. Heat Mass Tran.*, **49** (2006), 628–639. <https://doi.org/10.1016/j.ijheatmasstransfer.2005.07.049>
11. A. M. Megahed, Slip flow and variable properties of viscoelastic fluid past a stretching surface embedded in a porous medium with heat generation, *J. Cent. Sou. Univ.*, **23** (2016), 991–999. <https://doi.org/10.1007/s11771-016-3147-4>
12. W. Ibrahim, B. Hindebu, Magnetohydrodynamic (mhd) boundary layer flow of Eyring-Powell nanofluid past stretching cylinder with cattaneo-christov heat flux model, *Nonlinear Eng.*, **8** (2019), 303–317. <https://doi.org/10.1515/nleng-2017-0167>
13. M. Bilal, S. Ashbar, Flow and heat transfer analysis of Eyring-Powell fluid over stratified sheet with mixed convection, *J. Egypt. Math. Soc.*, **28** (2020), 40. <https://doi.org/10.1186/s42787-020-00103-6>
14. W. Abbas, A. M. Megahed, Powell-Eyring fluid flow over a stratified sheet through porous medium with thermal radiation and viscous dissipation, *AIMS Mathematics*, **6** (2021), 13464–13479. <https://doi.org/10.3934/math.2021780>
15. S. Pramanik, Casson fluid flow and heat transfer past an exponentially porous stretching surface in presence of thermal radiation, *Ain Shams Eng. J.*, **5** (2014), 205–212. <https://doi.org/10.1016/j.asej.2013.05.003>
16. S. Rana, R. Mehmood, N. S. Akbar, Mixed convective oblique flow of a casson fluid with partial slip, internal heating and homogeneous heterogeneous reactions, *J. Mol. Liq.*, **222** (2016), 1010–1019. <https://doi.org/10.1016/j.molliq.2016.07.137>
17. E. Alali, A. M. Megahed, MHD dissipative Casson nanofluid liquid film flow due to an unsteady stretching sheet with radiation influence and slip velocity phenomenon, *Nanotechnol. Rev.*, **11** (2022), 463–472. <https://doi.org/10.1515/ntrev-2022-0031>
18. T. Hayat, S. A. Shehzad, H. H. Al-Sulami, S. Asghar, Influence of thermal stratification on the radiative flow of Maxwell fluid, *J. Braz. Soc. Mech. Sci.*, **35** (2013), 381–389. <https://doi.org/10.1007/s40430-013-0036-8>
19. K. V. Prasad, K. Vajravelu, A. Sujatha, Influence of internal heat generation/absorption, thermal radiation, magnetic field, variable fluid property and viscous dissipation on heat transfer characteristics of a Maxwell fluid over a stretching sheet, *J. Appl. Fluid Mech.*, **6** (2013), 249–256. <https://doi.org/10.36884/JAFM.6.02.19525>

20. A. M. Megahed, Improvement of heat transfer mechanism through a Maxwell fluid flow over a stretching sheet embedded in a porous medium and convectively heated, *Math. Comput. Simulat.*, **187** (2021), 97–109. <https://doi.org/10.1016/j.matcom.2021.02.018>
21. M. I. Khan, A. Alsaedi, S. Qayyum, T. Hayat, M. I. Khan, Entropy generation optimization in flow of Prandtl-Eyring nanofluid with binary chemical reaction and Arrhenius activation energy, *Colloids Surf. A*, **570** (2019), 117–126. <https://doi.org/10.1016/j.colsurfa.2019.02.060>
22. M. I. Khan, F. Haq, S. A. Khan, T. Hayat, M. I. Khan, Development of thixotropic nanomaterial in fluid flow with gyrotactic microorganisms, activation energy, mixed convection, *Comput. Meth. Prog. Bio.*, **187** (2020), 105186. <https://doi.org/10.1016/j.cmpb.2019.105186>
23. T. Hayat, K. Muhammad, S. Momani, Melting heat and viscous dissipation in flow of hybrid nanomaterial: a numerical study via finite difference method, *J. Therm. Anal. Calorim.*, **147** (2022), 6393–6401. <https://doi.org/10.1007/s10973-021-10944-7>
24. C. I. Christov, On frame indifferent formulation of the Maxwell-Cattaneo model of finite-speed heat conduction, *Mech. Res. Commun.*, **36** (2009), 481–486. <https://doi.org/10.1016/j.mechrescom.2008.11.003>
25. T. Hayat, M. I. Khan, M. Farooq, A. Alsaedi, M. Waqas, T. Yasmeen, Impact of Cattaneo-Christov heat flux model in flow of variable thermal conductivity fluid over a variable thicked surface, *Int. J. Heat Mass Tran.*, **99** (2016), 702–710. <https://doi.org/10.1016/j.ijheatmasstransfer.2016.04.016>
26. T. Hayat, S. Qayyum, S. A. Shehzad, A. Alsaedi, Chemical reaction and heat generation/absorption aspects in flow of Walters-B nanofluid with Cattaneo-Christov double-diffusion, *Results Phys.*, **7** (2017), 4145–4152. <https://doi.org/10.1016/j.rinp.2017.10.036>
27. J. Z. Sui, L. C. Zheng, X. X. Zhang, Boundary layer heat and mass transfer with Cattaneo-Christov double-diffusion in upper-convective Maxwell nanofluid past a stretching sheet with slip velocity, *Int. J. Therm. Sci.*, **104** (2016), 461–468. <https://doi.org/10.1016/j.ijthermalsci.2016.02.007>
28. S. A. Shehzad, T. Hayat, A. Alsaedi, M. A. Meraj, Cattaneo-Christov heat and mass flux model for 3D hydromagnetic flow of chemically reactive Maxwell liquid, *Appl. Math. Mech.*, **38** (2017), 1347–1356. <https://doi.org/10.1007/s10483-017-2250-6>
29. K. S. Ullah, N. Ali, T. Hayat, Z. Abbas, Heat transfer analysis based on Cattaneo–Christov heat flux model and convective boundary conditions for flow over an oscillatory stretching surface, *Therm. Sci.*, **23** (2019), 443–455. <https://doi.org/10.2298/TSCI160225172U>
30. R. Garia, S. K. Rawat, M. Kumar, M. Yaseen, Hybrid nanofluid flow over two different geometries with Cattaneo-Christov heat flux model and heat generation: A model with correlation coefficient and probable error, *Chinese J. Phys.*, **74** (2021), 421–439. <https://doi.org/10.1016/j.cjph.2021.10.030>
31. T. Hayat, K. Muhammad, A. Alsaedi, Melting effect and Cattaneo-Christov heat flux in fourth-grade material flow through a Darcy-Forchheimer porous medium, *Appl. Math. Mech.*, **42** (2021), 1787–1798. <https://doi.org/10.1007/s10483-021-2798-6>
32. M. A. A. Mahmoud, Chemical reaction and variable viscosity effects on flow and mass transfer of a non-Newtonian visco-elastic fluid past a stretching surface embedded in a porous medium, *Meccanica*, **45** (2010), 835–846. <https://doi.org/10.1007/s11012-010-9292-1>

33. A. M. Megahed, M. Gnaneswara Reddy, W. Abbas, Modeling of MHD fluid flow over an unsteady stretching sheet with thermal radiation, variable fluid properties and heat flux, *Math. Comput. Simulat.*, **185** (2021), 583–593. <https://doi.org/10.1016/j.matcom.2021.01.011>
34. S. H. Han, L. C. Zheng, C. R. Li, X. X. Zhang, Coupled flow and heat transfer in viscoelastic fluid with Cattaneo-Christov heat flux model, *Appl. Math. Lett.*, **38** (2014), 87–93. <https://doi.org/10.1016/j.aml.2014.07.013>
35. A. Rauf, Z. Abbas, S. A. Shehzad, A. Alsaedi, T. Hayat, Numerical simulation of chemically reactive Powell-Eyring liquid flow with double diffusive Cattaneo-Christov heat and mass flux theories, *Appl. Math. Mech.*, **39** (2018), 467–476. <https://doi.org/10.1007/s10483-018-2314-8>
36. A. M. Megahed, Steady flow of MHD Williamson fluid due to a continuously moving surface with viscous dissipation and slip velocity, *Int. J. Mod. Phys. C*, **31** (2020), 2050019. <https://doi.org/10.1142/S0129183120500199>
37. A. M. Megahed, Williamson fluid flow due to a nonlinearly stretching sheet with viscous dissipation and thermal radiation, *J. Egypt. Math. Soc.*, **27** (2019), 12. <https://doi.org/10.1186/s42787-019-0016-y>
38. H. I. Andersson, Slip flow past a stretching surface, *Acta Mech.*, **158** (2002), 121–125. <https://doi.org/10.1007/BF01463174>



AIMS Press

©2022 the Author(s), licensee AIMS Press. This is an open access article distributed under the terms of the Creative Commons Attribution License (<http://creativecommons.org/licenses/by/4.0>)